Communication

Connectivity of Phases and Growth Mechanisms in Peritectic Alloys Solidified at Low Speed: an X-Ray Tomography Study of Cu-Sn

M. RAPPAZ, F. KOHLER, J. VALLOTON, A.B. PHILLION, and M. STAMPANONI

The variety of microstructures that form at low solidification speed in peritectic alloys, bands, and islands, or even coupled (or cooperative) growth of the primary α and peritectic β phases, have been previously explained by nucleation-growth mechanisms. In a recent investigation on Cu-Sn, a new growth mechanism was conjectured on the basis of two-dimensional (2-D) optical microscopy and electron backscattered diffraction (EBSD) observations made in longitudinal sections. In the present contribution, synchrotron-based tomographic microscopy has been used to confirm this mechanism: α and β phases totally interconnected in three dimensions and bands (or islands) can result from an overlay mechanism, rather than from a nucleation events sequence. When the lateral growth of a new layer is too fast, an instability can lead to the formation of a lamellar structure as for eutectic alloys.

M. RAPPAZ, Professor, J. VALLOTON, Ph.D. Student, and A.B. PHILLION, NSERC Postdoctoral Fellow, are with the Computational Materials Laboratory, Ecole Polytechnique Fédérale de Lausanne, CH-1015 Lausanne, Switzerland. Contact e-mail: michel.rappaz@epfl.ch F. KOHLER, formerly Ph.D. Student, Computational Materials Laboratory, Ecole Polytechnique Fédérale de Lausanne, is Tribology R&D Engineer, ETA SA Manufacture, Hologère Suisse, CH-2540 Grenchen, Switzerland. M. STAMPANONI, Assistant Professor for X-ray Microscopy and Head of the Tomography Group, ETH Zürich, CH-8092 Zürich, Switzerland, is with the Paul Scherrer Institut, Swiss Light Source, CH-5323 Villigen, Switzerland.
Manuscript submitted September 18, 2009.
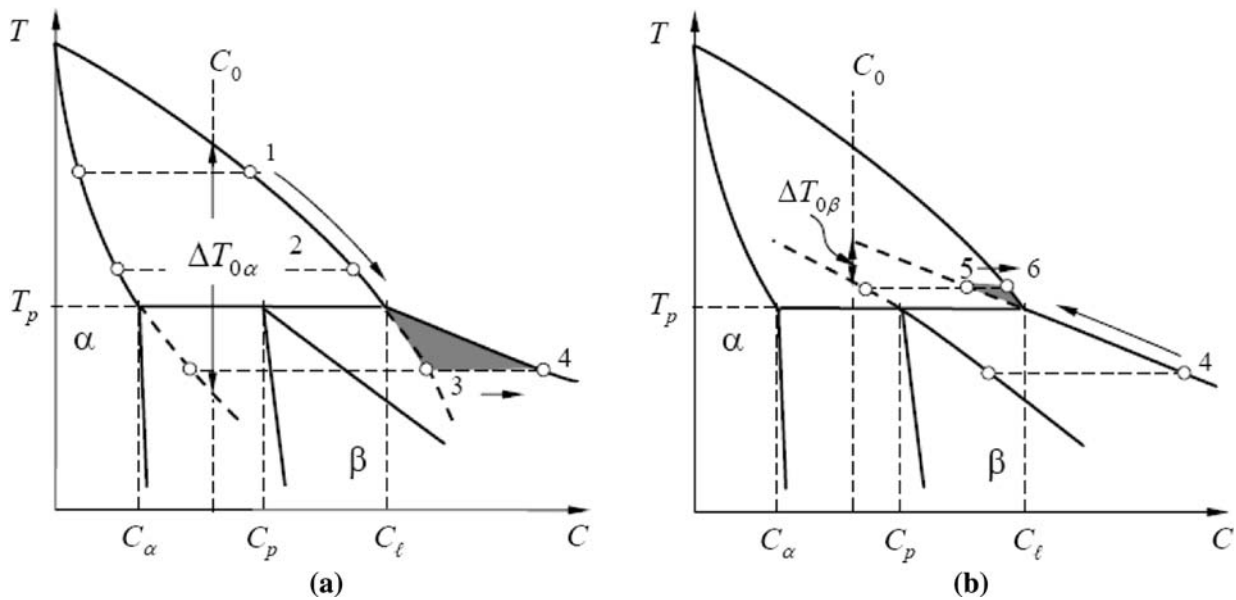Article published online January 5, 2010.

Steel, bronze, brass, and many other commercially important alloys exhibit peritectic transitions during solidification.[1] This invariant reaction in binary alloys is characterized by the transformation of two phases, liquid (l) and primary (α), into the peritectic phase (β), at temperature T_p and peritectic composition C_p (Figure 1). In the hypoperitectic region, i.e., for a nominal composition of alloy C_0 such that $C_\alpha < C_0 < C_p$, a number of different microstructures have been observed during directional solidification at low growth rate in an imposed thermal gradient G.[2] By low growth rate, we mean a growth velocity V such that a planar front of the α phase would be stable, should the peritectic phase not be present. This condition is met when

$$V < V_{\text{crit}} = \frac{GD_l}{\Delta T_{0\alpha}}$$

where G is the thermal gradient, D_l is the diffusion coefficient of the solute element in the liquid phase, and $\Delta T_{0\alpha}$ is the solidification interval of the α phase.

The diversity of microstructures obtained when $C_\alpha < C_0 < C_p$ and $V < V_{\text{crit}}$ is due to an inherent instability of both the α- and the β-planar fronts. Figure 1 illustrates schematically why neither of these phases is stable under such conditions. Neglecting any nucleation undercooling, the first solid to form under directional solidification is α with a composition $k_{0\alpha} C_0$, where $k_{0\alpha}$ is the partition coefficient for the α phase. In the transient to steady state, the α solid grows with a planar front morphology while the interfacial liquid composition $C_1^{*\alpha}$ increases from C_0 to $C_0/k_{0\alpha}$ (points labeled (1) through (3) in Figure 1). Concurrently, the interface temperature moves from the liquidus, $T_{\text{liq}}^\alpha(C_0)$, to the solidus of α, $T_{\text{sol}}^\alpha(C_0) = T_{\text{liq}}^\alpha(C_0/k_{0\alpha})$. However, as soon as $C_1^{*\alpha}$ goes beyond $C_1 = C_1(T_p)$, the liquid becomes undercooled with respect to β (gray area in Figure 1(a)), since the liquidus of α is below that of β. Therefore, the peritectic phase can nucleate and grow ahead of the primary phase.[3–5] If the β phase entirely covers the primary phase and prevents it from further growth, this gives rise to a band of β covering the previous α solid.

Considering now the growth of a β-planar front starting at point (4) (Figure 1(b)), the solid composition C_β^* is larger than C_0. Therefore, the interfacial composition has to decrease in order to reach a steady-state β-planar front growth (points (4) through (5)). At some point, the liquid interfacial composition falls below $C_1(T_p)$. This liquid is now undercooled with respect to α (gray area in Figure 1(b)), allowing then the α phase to nucleate and grow ahead of the β phase (point labeled (6)). As the loop shown in Figure 1 (points (1) through (6)) can start again, this sequence of α- and β-phase nucleation-growth events leads to an alternation of α and β bands perpendicular to the thermal gradient G.

Such bands have been observed in longitudinal sections of Fe-Ni alloys,[3,6] and more recently in the Cu-Sn system.[7] A nucleation and constitutional undercooling criterion has also been developed, by Hunziker et al.,[8] to predict the appearance of these bands based on the critical undercoolings for the nucleation of the α and β phases. However, when the lateral spreading of a new phase in a direction perpendicular to G over the pre-existing front growing in the direction of G is considered, together with the solute field interactions near the triple junction $\alpha - l - \beta$,[5,9,10] incomplete coverage of one phase over the other may occur. This leads to the formation of islands, which are therefore like incomplete bands. When convection is present, interconnected treelike microstructures, appearing almost as bands in longitudinal sections, have also been observed and modeled by Mazumder et al.[11]

Finally, another interesting microstructure that can form in peritectic alloys at low growth rate is the

Fig. 1—Schematic diagram of (*a*) the α-planar front growth leading to an undercooled liquid with respect to the β phase, and (*b*) the β-planar front growth leading to an undercooled liquid with respect to the α phase.

simultaneous growth of α- and β-lamellae in the direction of the thermal gradient G. Although similar to the well-known coupled growth of eutectic alloys, the α- and β-lamellae of peritectic alloys both reject solute elements ahead of the interface. Less solute is rejected by the β-phase since $k_{0\beta} > k_{0\alpha}$. Predicted in 1959 by Chalmers,[12] coupled (or cooperative) growth in peritectic alloys was first observed in Ni-Al, by Lee and Verhoeven,[13] and then in Fe-Ni by Kurz and co-workers.[6,14] As shown by directional solidification experiments and multiphase field simulations,[6,10,15–17] lamellae structures can start growing from islands, providing the distance separating the islands falls within a range of stable lamellar spacings.[10]

The observations of bands, islands, and cooperative lamellae growth in peritectics was limited up to now to small solidification interval alloys, typically with $\Delta T_{0\alpha} < 10$ K. Surprisingly, none of the previous investigations tried to determine if the bands, islands, and lamellae of the two phases had a crystallographic relationship, *e.g.*, by using electron backscattered diffraction (EBSD). In a recent contribution, Kohler *et al.*[7] investigated peritectic solidification in the Cu-Sn system, an alloy with a solidification interval $\Delta T_{0\alpha}$ nearly 50 times that of Fe-Ni in the hypoperitectic region (around 120 K near C_p). Using a Bridgman solidification setup with quench, in which solutal convection was minimized by having small specimen dimensions, these authors observed all three of the peritectic microstructures discussed previously: lamellae, bands, and islands. The crystallographic orientations of the resulting microstructures were also investigated.

An example micrograph from the work of Kohler *et al.*[7] is shown in Figure 2 for a Cu-21 wt pct Sn specimen solidified at 0.58 μm/s in a cylinder (4/6 mm inner/outer diameter). In the top view of this longitudinal section micrograph, the α phase appears in light

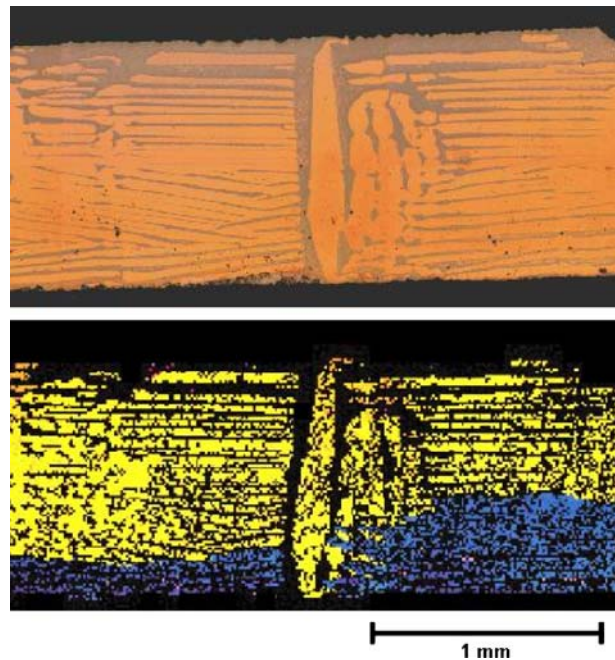Fig. 2—Longitudinal section of a Cu-21 wt pct Sn specimen solidified at $V = 0.58$ μm/s in a thermal gradient $G = 200$ K/cm. The top view shows the microstructure with α and β in light brown and bluish brown, respectively. The bottom view shows an EBSD false color.

brown while the β phase is colored in blueish brown. The solidification direction goes from left to right. As can be seen, there is a transition in growth from lamellae to bands and then back to lamellae. The transition from bands to lamellae on the right-hand side clearly goes through an intermediate stage of semicontinuity and then partial bands or islands. In the bottom view, a

reconstructed false color micrograph obtained from the EBSD measurements is shown. Due to a solid-state transformation of β either into ($\delta + \alpha$) *via* a eutectoid reaction or into a martensitic phase, only the α phase could be indexed. As can be seen, the α phase in this section is made of two grains, yellow and blue. More importantly, within a grain, the same orientation is measured for the lamellae on the left and the right sides of the micrograph and is not lost when discrete bands form in the middle of the longitudinal section.

These observations can be explained by one of two mechanisms: (1) the whole structure is in fact continuous in three dimensions but may appear as discontinuous discrete bands in two-dimensional (2-D) metallographic sections; and (2) when a new phase nucleates ahead of an existing one, there is a systematic coherency relationship. Of these two mechanisms, the second mechanism can be immediately ruled out, although a Kurdjumov–Sachs crystallographic relationship was observed between the fcc-α and bcc-β phases in another region of the specimen where the β phase did not transform and could be indexed.[7] There are indeed 24 such relationships between the $\{100\}_\alpha$ and $\{110\}_\beta$ reference systems. In the first mechanism, a new band of a phase, say, β, does not require any nucleation event at the $\alpha - 1$ interface if it exists already in another region
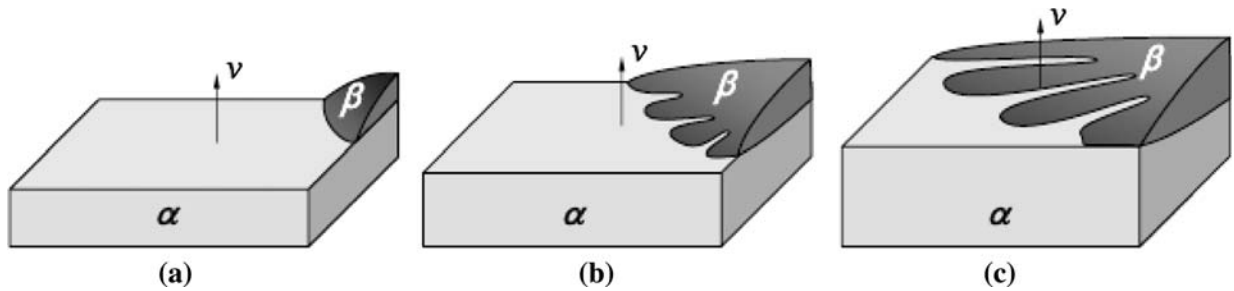

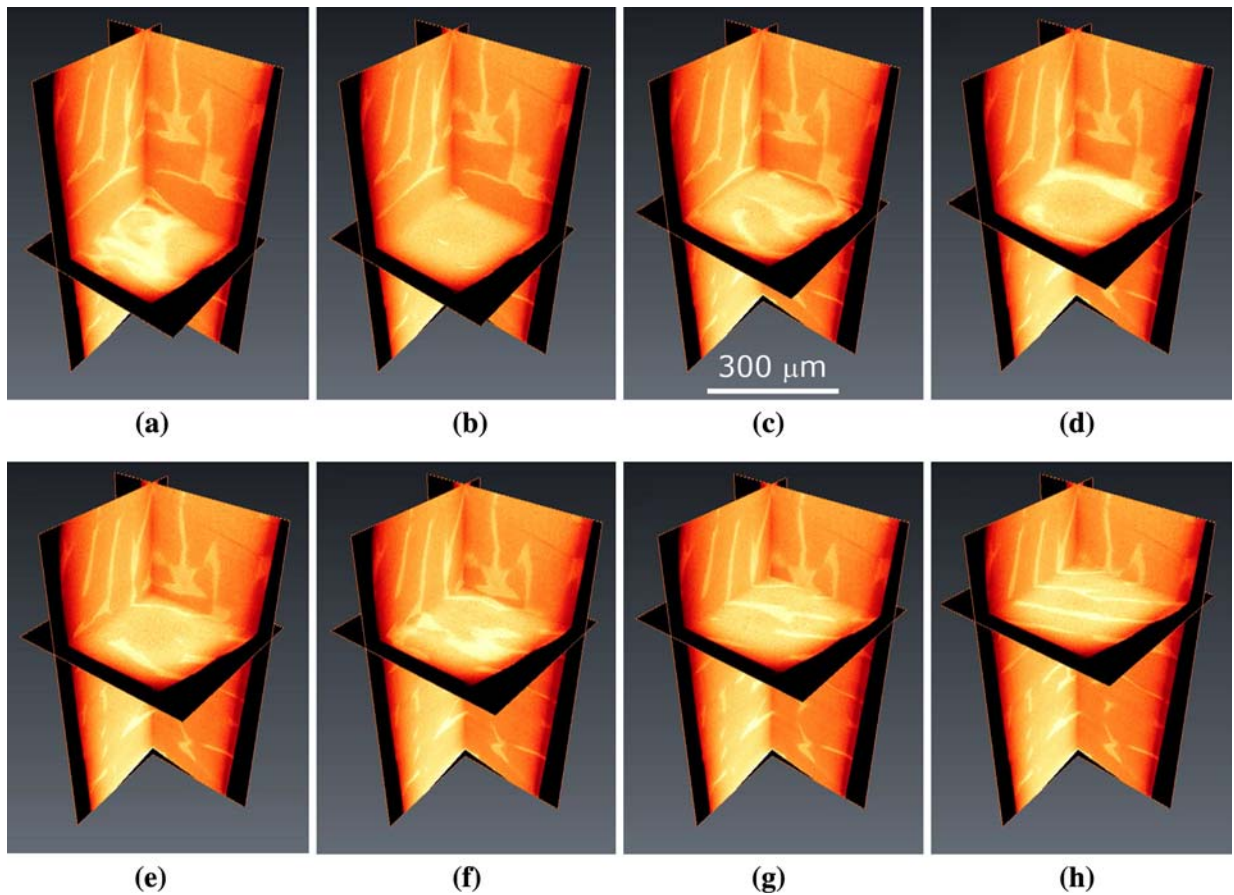Fig. 3—Schematic of the overlay growth mechanism of one phase (in this case, β) over a planar front of α.[7,20]

Fig. 4—Virtual, orthogonal slices obtained with synchrotron-based tomographic microscopy of the α (dark brown) and β (brown-yellow) microstructure in a region of the specimen shown in Fig. 2, where bands (in (b)) are destabilized and give rise to a lamellae structure (in (h)). The thermal gradient G is vertical and up.

of the specimen. The new phase β can then simply grow laterally from this region since the liquid ahead of the $\alpha - 1$ exhibits the largest supersaturation. This *overgrowth* or *overlay mechanism*, which is of course not possible in two dimensions, is shown schematically in Figure 3. As lateral growth of one phase over the other occurs in a nearly nil (horizontal) thermal gradient and at a velocity that can be much higher than the pulling velocity V of the specimen, it can be unstable (Figure 3). It then develops β cells. Since the α phase is still growing in between the spaces left by the β cells, an alternate sequence of the primary and peritectic phases is formed and a cooperative growth is thus initiated between the α and β phases, leading to the formation of a α-β lamellar structure. A similar situation can occur during the lateral propagation of an α-layer over a β-liquid interface. This mechanism is similar to that observed by Akamatsu *et al.*[19] on organic eutectic alloys at the onset of coupled growth.

In order to check the continuity of the α and β phases in three dimensions, and hence the validity of this growth mechanism, synchrotron-based tomographic microscopy experiments were carried out at the Tomcat beamline of the Swiss Light Source (Paul Scherrer Institute, Villigen, Switzerland)[21] on Cu-Sn specimens of 300-μm thickness extracted from the solidified cylinders. The energy of the X-ray beam was 38 keV, the voxel size was 0.74 μm, and the specimen-to-screen distance was 2 mm. The combination of high X-ray energy and small sample dimensions was necessary since both Cu and Sn are strong X-ray absorbers.

Figure 4 shows 8 three-dimensional (3-D) views of the microstructure from a subsection of the specimen shown in Figure 2, in a region where lateral overgrowth gave rise to the lamellar structure. The images are shown in reverse contrast with the α phase appearing in dark brown since it is leaner in Sn ($C_\alpha \approx 13.5$ wt pct), while the β phase appears brighter since $C_\beta \approx 22$ wt pct. In this series of images, the thermal gradient G is vertical; the evolution in microstructure is shown by two fixed vertical sections and one horizontal section that "moves" in the solidification direction from image (a) to image (h). Although this sequence was recorded postmortem, and not *in-situ* during growth of the microstructure, it shows the complexity of the phase interconnections. In some regions, *e.g.*, at midheight, the two longitudinal sections exhibit a band-type morphology. In others, *e.g.*, near the top of the left section, it is clearly lamellar. As shown by the moving horizontal section, the α phase is interconnected. While lateral growth of both phases appears to be not as smoothed as illustrated in Figure 3, it finally gives rise to a fairly regular arrangement of lamellae near the top of the specimen. As mentioned in References 7 and 18, solutal convection is probably responsible for the irregularities of the microstructure, especially during overgrowth. Convection not only gradually increases the average composition of the liquid during growth, due to macrosegregation, it also affects the local composition. Numerical simulations[18] revealed a complex, unsteady streamline pattern, with solute-enriched and solute-lean plumes of liquid going upward and downward,
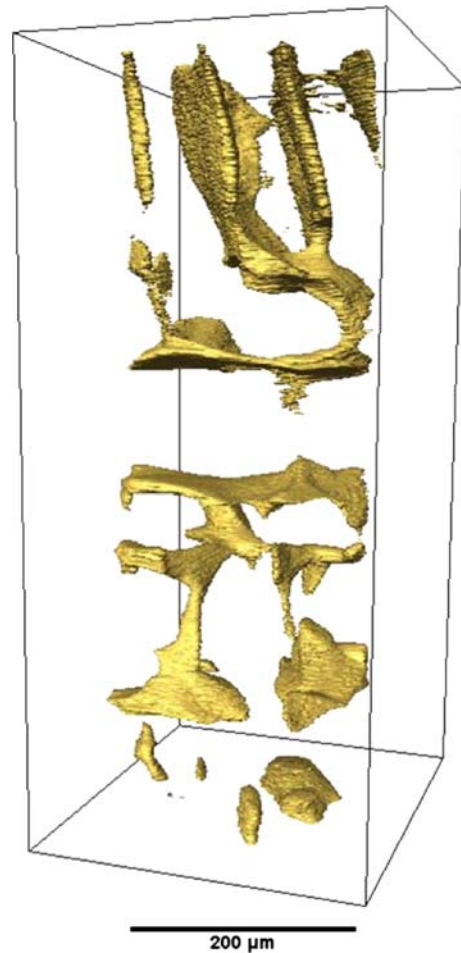

Fig. 5—3-D segmented view of the β phase in a region of the specimen shown in Fig. 2. The transition from lamellae to bands is evident. The thermal gradient G is vertical and up.

respectively, with a nonzero horizontal component of the velocity (*i.e.*, helicoidal movements).

The connectivity of the phases can also be seen in the 3-D image shown in Figure 5. In this figure, the α phase has been removed from the drawing, leaving only the interconnected β phase. The thermal gradient G is vertical and points up. As can be seen in the figure, the β phase goes through two distinct transitions. First, in the lower half of the image, there is a transition from a lamellae- to a band-type structure. Second, in the upper half of the image, there is the reverse transition, from bands to lamellae. These transitions, 3-D in nature, provide clear evidence supporting the growth overlay mechanism as a means of phase propagation. Although it might appear that the upper β region is separate from the lower one, and hence could be the result of a new nucleation event, it is believed that the two regions are in fact continuous and that the link between them occurs outside the bounding box of the X-ray tomographic scan.

Despite convection effects and solid-state transformations that make the analysis of the postmortem microstructure more difficult, X-ray tomographic observations have clearly shown the 3-D connectivity of the α and β phases during low speed growth of Cu-Sn alloys. These

observations explain the continuity of the grains measured previously by EBSD in 2-D sections and confirm that bands might form by an overgrowth mechanism of one phase over the other and do not require necessarily renucleation. If lateral growth is unstable, bands can give rise to lamellae in a similar fashion to the initial state of coupled eutectic growth. X-ray tomography also opens new opportunities for the study of peritectic solidification at low growth rate. In a first step, we plan to grow Cu-Sn alloys in capillaries of smaller dimensions (typically about 400-μm diameter) in order to further reduce convection and allow for 3-D characterization of the whole specimen. In a second step, we hope to perform direct *in-situ* X-ray tomography observations of Cu-Sn growth at low speed in a specifically designed furnace.

REFERENCES

1. H.W. Kerr and W. Kurz: *Int. Met. Rev.*, 1996, vol. 41, pp. 129–64.
2. W.J. Boettinger, S.R. Coriell, A.L. Greer, A. Karma, W. Kurz, M. Rappaz, and R. Trivedi: *Acta Mater.*, 2000, vol. 48, pp. 43–70.
3. R. Trivedi: *Metall. Mater. Trans. A*, 1995, vol. 26A, pp. 1583–90.
4. R. Trivedi, H. Miyahara, P. Mazumder, E. Simsek, and S.N. Tewari: *J. Cryst. Growth*, 2001, vol. 222, pp. 365–79.
5. R. Trivedi and J.S. Park: *J. Cryst. Growth*, 2002, vol. 235, pp. 572–88.
6. S. Dobler, T.S. Lo, M. Plapp, A. Karma, and W. Kurz: *Acta Mater.*, 2004, vol. 52, pp. 2795–2808.
7. F. Kohler, L. Germond, J.-D. Wagnière, and M. Rappaz: *Acta Mater.*, 2008, vol. 57, pp. 56–68.
8. O. Hunziker, M. Vandyoussefi, and W. Kurz: *Acta Mater.*, 1998, vol. 46, pp. 6325–36.
9. R. Trivedi, A. Karma, T.S. Lo, J.S. Park, and M. Plapp: *Solidification Microstructures*, Proc. 2nd Workshop, Zermatt, Switzerland, 1998.
10. T.S. Lo, S. Dobler, M. Plapp, A. Karma, and W. Kurz: *Acta Mater.*, 2003, vol. 51, pp. 599–611.
11. P. Mazumder, T. Trivedi, and A. Karma: *Metall. Mater. Trans. A*, 2000, vol. 31A, pp. 1233–46.
12. B. Chalmers: *Physical Metallurgy*, Wiley, New York, NY, 1959.
13. J.H. Lee and J.D. Verhoeven: *J. Cryst. Growth*, 1994, vol. 144, pp. 353–66.
14. M. Vandyoussefi, H.W. Kerr, and W. Kurz: *Acta Mater.*, 2000, vol. 48, pp. 2297–2306.
15. S. Dobler: PhD Thesis 2409, Ecole Polytechnique Fédérale de Lausanne, Lausanne, Switzerland, 2001, http://library.epfl.ch/theses/?nr = 2409.
16. S. Dobler and W. Kurz: *Z. Metallkd.*, vol. 95, pp. 592–95.
17. T.S. Lo, A. Karma, and M. Plapp: *Phys. Rev. E*, 2001, vol. 63, pp. 031504-1–031504-15.
18. F. Kohler: PhD Thesis 4027, Ecole Polytechnique Fédérale de Lausanne, Lausanne, Switzerland, 2008, http://library.epfl.ch/theses/?nr = 4037.
19. S. Akamatsu, S. Moulinet, and G. Faivre: *Metall. Mater. Trans. A*, 2001, vol. 32A, pp. 2039–48.
20. J.A. Dantzig and M. Rappaz: *Solidification*, EPFL Press, Lausanne, Switzerland, 2009.
21. M. Stampanoni, A. Groso, A. Isenegger, G. Mikuljan, Q. Chen, A. Bertrand, S. Henein, R. Betemps, U. Frommherz, P. Böhler, D. Meister, M. Lange, and R. Abela: *Developments in X-Ray Tomography V*, Proc. SPIE, U. Bonse, ed., vol. 6318, 63180M, (2006) 1605-7422/06, DOI:10.1117/12.679497.